

Urban area change detection based on generalized likelihood ratio test

Weiyang Zhao, Sylvain Lobry, Henri Maitre, Jean-Marie Nicolas, Florence Tupin
 LTCI, Télécom ParisTech, Université Paris-Saclay, 75013, Paris, France

Abstract—Change detection methods often use denoised data because the original speckle noise has a strong influence on the detection results. The effect of using different data sources (different equivalent number of looks, original data, denoised data) and different threshold methods are studied based on four kinds of generalized likelihood ratio test approaches. NL-SAR [1] denoised data and the corresponding spatially varying equivalent number of looks are taken into account in the detection procedure. The bi-temporal experimental results on simulated data, realistic synthetic SAR data and Sentinel-1 SAR data show the improvement of using equivalent number of looks of denoised data and corresponding adaptive thresholds for change detection in urban areas.

I. INTRODUCTION

Synthetic aperture radar (SAR) imagery has the main advantage of being an all-time and all-weather sensor, with a very good accuracy for the acquisition geometry. With abundant spatial and temporal information, SAR images have been widely used to monitor changes on the Earth surface, such as urban change detection, environment monitoring and database updating [2]. The recent launch of Sentinel sensors will provide long term time series, well adapted for urban monitoring. It is well known that the developments of urban areas will cause plenty of changes: appearing and disappearing objects as well as cross changes between these two change types. Many approaches have been proposed for SAR change detection. Binary and multi-temporal SAR change detection methods are mainly based on likelihood ratio [3]–[6], image ratio [6], coherence [7], image texture and structure analysis [8]. Due to the specific noise and statistics of coherent SAR images, likelihood ratio tests are often used.

In this paper, urban area changes are studied using generalized likelihood ratio test statistic approaches, which are based on original [3] or denoised data [4], and described in next section. Our aim is to study the interest of the denoising step and the influence of the equivalent number of looks (ENL) in the change detection procedure. To compare these methods, they were applied to process simulated data, realistic synthetic data and real Sentinel-1 SAR data, and using NL-SAR as the denoising method.

II. COMPARISON OF CHANGE DETECTION METHODS

This section mainly introduces the denoising method of NL-SAR [1], the different variants of GLRT and threshold approaches. The notations that will be intensively used in the following are:

y, y_1, y_2 : pixel values of the intensity data.

u, u_1, u_2, u_{12} : noise free values of the intensity data.

$\hat{u}, \hat{u}_1, \hat{u}_2$: estimated values of the noise free values or pixel values of the denoised intensity data.

$\hat{u}_1^{ML}, \hat{u}_2^{ML}, \hat{u}_{12}^{ML}$: maximum likelihood estimated data.

L, L_1, L_2 : original equivalent number of looks (ENL).

\hat{L}_1, \hat{L}_2 : ENL of the denoised data, corresponding to \hat{u}_1, \hat{u}_2 respectively.

A. Denoising approaches and NL-SAR

Speckle noise is an inherent problem in SAR imaging. It is due to coherent processing of backscattered signals from multiple distributed targets, and bring difficulties for image interpretation. So, a multi-look processing, which usually leads to an image resolution reduction, is often applied as a preliminary step. Preservation of point-like, fine structures and textures requires to locally adapt the despeckling process. Non-local means compute data-driven weights from the similarity between small image patches and adapt to sample selection to denoise the image. NL-SAR is a SAR adapted version of this method, with automatic parameter adjustment. Starting from an input value y_i for pixel i , this method gives the output of a denoised value \hat{u}_i and an associated equivalent number of looks \hat{L}_i [1]. Other denoising method could be used provided that they associate an ENL to the denoised result.

B. Generalized likelihood ratio test (GLRT)

In statistics, change detection can be considered as a comparison of two hypotheses H_0 and H_1 , which correspond to the null and alternative hypothesis respectively.

H_0 : $u_1 = u_2 = u_{12}$ (no change)

H_1 : $u_1 \neq u_2$ (change)

The likelihood ratio test is based on the likelihood ratio of the observations y_1, y_2 , which is defined as:

$$LRT(y_1, y_2) = \frac{P(y_1, y_2 | u_{12}, H_0)}{P(y_1 | u_1, H_1)P(y_2 | u_2, H_1)} \quad (1)$$

where u_1 and u_2 are the noise free intensity values corresponding to y_1 and y_2 with associated ENL L_1 and L_2 . Considering the L look intensity data follows the Gamma distribution, we have

$$P(y | u) = \frac{L^L}{\Gamma(L)} \frac{y^{L-1}}{u^L} \exp\left(-\frac{Ly}{u}\right) \quad (2)$$

Since u_1, u_2 and u_{12} are not available, they can be replaced by their maximum likelihood estimations under H_0 and H_1 : $\hat{u}_1^{ML} = y_1, \hat{u}_2^{ML} = y_2, \hat{u}_{12}^{ML} = \frac{L_1 y_1 + L_2 y_2}{L_1 + L_2}$.

Then, the generalized likelihood ratio test is given by:

$$GLRT = (L_1 + L_2)^{L_1+L_2} \frac{(y_1)^{L_1}(y_2)^{L_2}}{(L_1 y_1 + L_2 y_2)^{L_1+L_2}} \quad (3)$$

by putting $\rho = \frac{y_1}{y_2}$,

$$GLRT = (L_1 + L_2)^{L_1+L_2} \frac{(\rho)^{L_1}}{(L_1 \rho + L_2)^{L_1+L_2}} \quad (4)$$

Since the distribution of ρ is known (the ratio of 2 Gamma distributed random variables follows a Fisher distribution [5]), it is possible to compute the GLRT probability density function (pdf).

GLRT change criterion can be used in different ways [3]–[5] which are discussed in section D.

C. GLRT combining noisy and denoised values

In this section, we suppose that we have a denoised value \hat{u}_i for each pixel corresponding to a denoising process and we investigate how to introduce this information and its associated ENL \hat{L}_i to GLRT.

AGLRT [4] (approximation of GLRT) defined by replaces the "true" values u_i by the denoised values. It does not take into account the different ENL of the denoised values. CGLRT [4] (GLRT extended to noisy and denoised data) takes into account the different ENL for each pixel, but the change detection threshold is difficult to adapt and is fixed globally. It is possible to compute the GLRT starting from the denoised observed values \hat{u}_i (it will be denoted by DGLRT).

1) *AGLRT (approximate GLRT)*: A joint way following [4] is to simply replace the unknown u_1, u_2 and u_{12} by \hat{u}_1, \hat{u}_2 and $\frac{\hat{u}_1 + \hat{u}_2}{2}$. It does not take into account the ENL.

$$AGLRT(y_1, y_2, \hat{u}_1, \hat{u}_2) = \frac{P(y_1, y_2 | u_{12}, H_0)}{P(y_1, y_2 | \hat{u}_1, \hat{u}_2, H_1)} \quad (5)$$

$$AGLRT(y_1, y_2, \hat{u}_1, \hat{u}_2) = \left[\frac{1}{4} \left(\frac{\hat{u}_2}{\hat{u}_1} + \frac{\hat{u}_1}{\hat{u}_2} + 2 \right) \right]^{-L} \exp \left[L \left(\frac{y_1}{\hat{u}_1} + \frac{y_2}{\hat{u}_2} - \frac{2(y_1 + y_2)}{\hat{u}_1 + \hat{u}_2} \right) \right] \quad (6)$$

2) *DGLRT (denoised GLRT)*: The denoised values \hat{u}_1 and \hat{u}_2 with associated ENL \hat{L}_1 and \hat{L}_2 are used instead of the intensity values y_1 and y_2 .

$$DGLRT(\hat{u}_1, \hat{u}_2) = \frac{P(\hat{u}_1, \hat{u}_2 | u_{12}, H_0)}{P(\hat{u}_1 | u_1, H_1) P(\hat{u}_2 | u_2, H_1)} \quad (7)$$

In this case, it equivalent to Eq. (3), but replacing y_1 and y_2 by \hat{u}_1 and \hat{u}_2 , and L_1 and L_2 by \hat{L}_1 and \hat{L}_2 . The generalized likelihood ratio test changed to be:

$$DGLRT = (\hat{L}_1 + \hat{L}_2)^{\hat{L}_1 + \hat{L}_2} \frac{(\hat{u}_1)^{\hat{L}_1} (\hat{u}_2)^{\hat{L}_2}}{(\hat{L}_1 \hat{u}_1 + \hat{L}_2 \hat{u}_2)^{\hat{L}_1 + \hat{L}_2}} \quad (8)$$

3) *CGLRT (combined GLRT)*: In this approach, both the original and denoised data are taken into account in the likelihood probability of H_0 and H_1 as $P(y_1, y_2, \hat{u}_1, \hat{u}_2 | H_0)$ and $P(y_1, y_2, \hat{u}_1, \hat{u}_2 | H_1)$.

The likelihood ratio test is given by:

$$CGLRT(y_1, y_2, \hat{u}_1, \hat{u}_2) = \frac{P(y_1, \hat{u}_1 | u_{12}, H_0) P(y_2, \hat{u}_2 | u_{12}, H_0)}{P(y_1, \hat{u}_1 | u_1, H_1) P(y_2, \hat{u}_2 | u_2, H_1)} \quad (9)$$

The maximum likelihood estimation of u_{12}, u_1, u_2 are given as follows:

$$\hat{u}_1^{ML} = \frac{Ly_1 + \hat{L}_1 \hat{u}_1}{L + \hat{L}_1} \quad (10)$$

$$\hat{u}_2^{ML} = \frac{Ly_2 + \hat{L}_2 \hat{u}_2}{L + \hat{L}_2} \quad (11)$$

$$\hat{u}_{12}^{ML} = \frac{Ly_1 + Ly_2 + \hat{L}_1 \hat{u}_1 + \hat{L}_2 \hat{u}_2}{2L + \hat{L}_1 + \hat{L}_2} \quad (12)$$

In the case of Gamma distribution with different number of looks, each probability term in $CGLRT(y_1, y_2)$ equation can be approximated under conditional independence assumption.

Then, the change criterion boils down to:

$$CGLRT(y_1, y_2) = \left(\frac{Ly_1 + \hat{L}_1 \hat{u}_1}{L + \hat{L}_1} \right)^{L + \hat{L}_1} \left(\frac{Ly_2 + \hat{L}_2 \hat{u}_2}{L + \hat{L}_2} \right)^{L + \hat{L}_2} \left(\frac{2L + \hat{L}_1 + \hat{L}_2}{Ly_1 + Ly_2 + \hat{L}_1 \hat{u}_1 + \hat{L}_2 \hat{u}_2} \right)^{2L + \hat{L}_1 + \hat{L}_2} \quad (13)$$

TABLE I
DIFFERENT GENERALIZED LIKELIHOOD RATIO TEST METHODS SUMMARY

| Methods | Used data | Equation |
|---------|---|----------|
| GLRT | y_1, y_2, L_1, L_2 | Eq.(4) |
| AGLRT | $y_1, y_2, \hat{u}_1, \hat{u}_2, L$ | Eq.(6) |
| DGLRT | $\hat{u}_1, \hat{u}_2, \hat{L}_1, \hat{L}_2$ | Eq.(8) |
| CGLRT | $y_1, y_2, \hat{u}_1, \hat{u}_2, L, \hat{L}_1, \hat{L}_2$ | Eq.(13) |

D. Exploiting GLRT and threshold choice

GLRT changed criterion threshold are usually defined using a quantile approach. Using the distribution of the change criterion under H_0 hypothesis (no change), it is possible to compute the threshold corresponding to a given false alarm probability (Pfa). It corresponds to a quantile of the distribution.

1) *Analytical distribution*: In the case of Eq.(4), it is possible to compute the distribution of ρ (ratio of 2 Gamma distribution random variables). It is thus possible to compute the pdf of GLRT(ρ) and the quantiles under H_0 (leading to a Meijer function for the cumulative distribution function [9]). The acquired value of the function given a false alarm rate α is then used as threshold for the change detection step.

For GLRT and DGLRT, it is thus possible to compute the thresholds analytically. For each values of the parameters L_1 and L_2 , a threshold is associated.

2) *Empirical learning of the distribution*: However, it's hard to obtain the distribution of AGLRT and CGLRT. Because these methods use both the noisy images and the denoised images. Therefore, we use Monte Carlo simulations to obtain empirical distributions.

Taking CGLRT change criterion for example, its pdf is computed using Monte Carlo simulations under the no change hypothesis (H_0 case). Then the thresholds (depending on L , L_1 and L_2) are computed for a fixed value (α), with $\tau^{CGLRT} = \text{quantile}(CGLRT, \alpha)$ [4]. The bigger the difference between the ENL, the smaller are the adaptive thresholds.

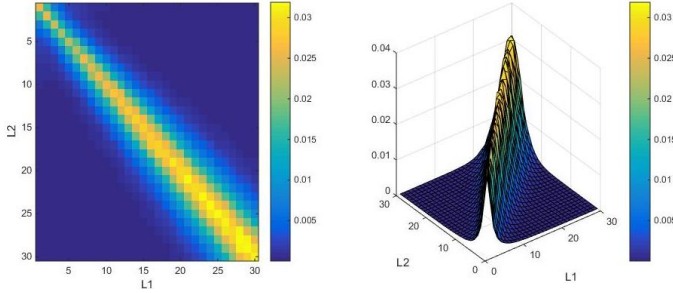


Fig. 1. Threshold values (example) obtained by Monte Carlo simulations for CGLRT with a false alarm rate of 1%. (2D and 3D threshold display)

III. DATA

In this part, we study the change detection performance of the change criterion on synthetic (toy images and realistic data) and real SAR data.

A. Synthetic data

Two intensity images with 10 different background values and targets are simulated, with $\mu_{target} = 1600$ and $\mu_{target} / \mu_{back}$ vary from 2 to 20. μ_{target} value was chosen according to the real value of buildings in a Sentinel-1 SAR image. Then, the noise free intensity images are multiplied by Gamma distributed noise. $y = m_{pure}S$, with m_{pure} the image without noise, S the Gamma random noise and y the acquired intensity data.

For the first and second background region of the simulated images, the $\mu_{target} / \mu_{back}$ in the noise free images are 2 and 4. So the changed points in these areas are hard to be detected.

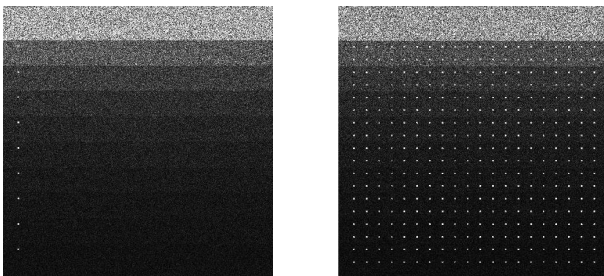


Fig. 2. Toy images used for change detection. Artificial targets with known values are added. Only the first points in 10 different background are not changed, as shown in the left (left). And all the other points appeared in the second image (right).

B. Realistic synthetic data

In this section, a realistic SAR image is simulated and then changes are applied.

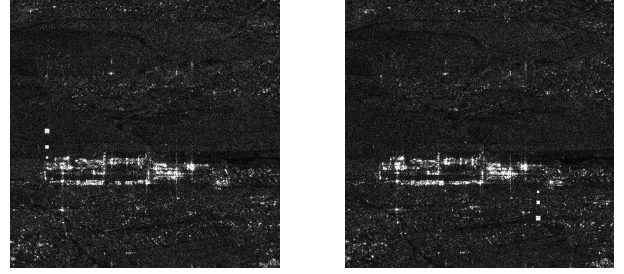


Fig. 3. Realistic synthetic image 1 and 2. The background image is obtained from an average of 49 Sentinel-1 images. The values of the changed areas were chosen based on the building's backscattering values in the real SAR image. The changed areas have different sizes with different backgrounds, and appearing and disappearing changed types.

To have an almost despeckled image (49 looks), the arithmetic mean of 49 Sentinel-1 intensity images is computed (m_I). Then, an image with changes is computed by introducing new objects. Two images are finally obtained through multiplying them by speckle noise.

Man-made structures such as buildings, fences or transmission towers produce very strong back-scattering. They usually have big intensities for some geometric configurations [10]. To control the real changed areas in the SAR images, several changed patches were added in the images, corresponding to isolated buildings with rectangular shape.

C. Sentinel-1 SAR images

The Sentinel-1 mission comprises a constellation of two polar-orbiting satellites, operating day and night performing C-band SAR imaging. The constellation will cover the entire world's land masses on a bi-weekly basis. In this paper, 2 Sentinel-1 images are used for the building area change detection. The registered 2 Sentinel-1 SAR images (resolution: 2.7x22 m to 3.5x22 m) over Paris Saclay area were obtained at 05/01/2015 and 18/01/2017, and they cover the same area as the SAR data used for creating the realistic synthetic image.

IV. RESULTS AND DISCUSSION

A. Change detection results comparison based on simulated data

To compare these methods and find the influence of ENL on the detection results, a denoising for the data is first applied, then the different change criteria are computed. After NL-SAR denoising, the ENL is larger in homogeneous areas than that of near geometrical structures. Point-like structures have the smallest ENL [1].

The detected results are significantly improved after using NL-SAR denoised data. AGLRT method does not use the ENL of denoised images, which makes this method has worse results comparing with DGLRT and CGLRT. CGLRT method combining both the noisy and denoised information got the best results.

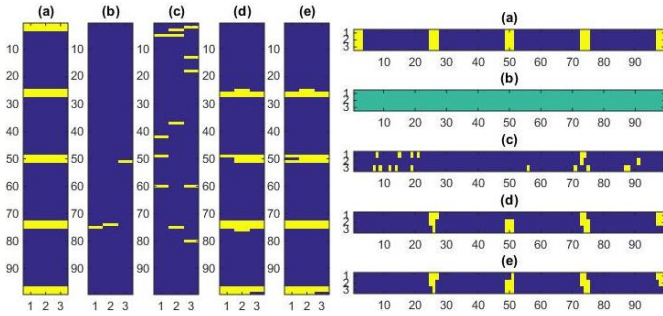


Fig. 4. Visual results (partial) comparison with $\alpha = 0.002$. (a) Change reference map. The vertical distributed patches are located in the last column from the second row to the sixth row (Fig.2). The horizontal patches are situated in the fourth row. (b) GLRT detection results. (c) AGLRT detection results. (d) DGLRT detection results. (e) CGLRT detection results.

B. Test on realistic synthetic data

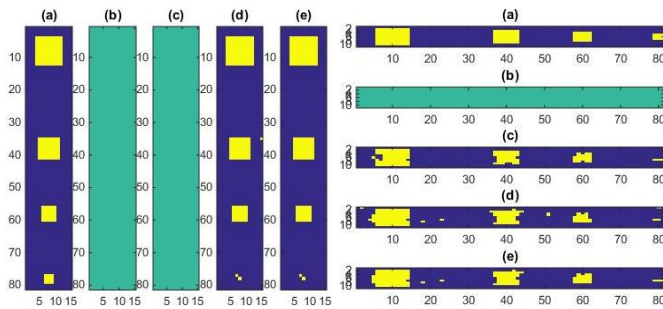


Fig. 5. Visual results (partial) comparison with $\alpha = 0.002$. The thresholds are computed using empirical quantile method for each pixel. The left side corresponding to disappearing patches, the right side corresponding to appearing patches. (a) Ground truth. (b) GLRT detection results. (c) AGLRT detection results. (d) DGLRT detection results. (e) CGLRT detection results.

Using adaptive threshold and taking into account the pixel ENL, DGLRT and CGLRT detection results are always better than that of AGLRT. It seems that AGLRT method is not good at detecting disappearing points. GLRT, which is applied only on the noisy values, nearly couldn't detect these kinds of changes.

All the change detection methods boil on the smallest patches. It's because the denoised data lost tiniest details and the edges are slightly jagged after processing by NL-SAR method. For the bigger patches, most of the changed points were detected by DGLRT and CGLRT methods which used the ENL. Building area changes belong to object changes which contents lots of changed points. After NL-SAR denoising, the ENL of these changed points will be changed significantly. Using the ENL will add more information to the change detection decision, and it will help the method getting better detected results.

C. Test on real SAR data

Based on above experimental results, the generalized likelihood methods were used to process the real SAR data with $\alpha = 0.002$. Satisfying change detection results were obtained by DGLRT and CGLRT methods.

Contrary to [4], in this paper we used an adaptive threshold taking into account \hat{L}_1 and \hat{L}_2 for each pixel learnt with Monte Carlo simulations as explained in the second section.

V. CONCLUSION

This paper has presented the influence of the equivalent number of looks (ENL) in the generalized likelihood ratio test change detection procedure. The ENL of the denoised data is taken into account, and adds more information for the change decision making.

We firstly analyzed different kinds of generalized likelihood ratio test methods (GLRT, AGLRT, DGLRT, CGLRT), which used different data, such as original data, denoised data, ENL of original data or denoised data. Then, the change detection results are compared based on simulated data, synthetic Sentinel-1 SAR data and Sentinel-1 SAR data. The bi-temporal experimental results shown that using the ENL of the NL-SAR denoised data and adaptive threshold could improve the change detection results. The future work will be focused on the multi-temporal Sentinel-1 SAR data analysis.

REFERENCES

- [1] C.A. Deledalle, Tupin Denis, L., Reigber F., and M. A. and Jäger. NL-SAR: A unified nonlocal framework for resolution-preserving (Pol)(In) SAR denoising. *IEEE Transactions on Geoscience and Remote Sensing*, 53(4):2021–2038, 2015.
- [2] C. Marin, F. Bovolo, and L. Bruzzone. Building change detection in multitemporal very high resolution SAR images. *IEEE Transactions on Geoscience and Remote Sensing*, 53(5):2664–2682, 2015.
- [3] P. Lombardo and T. Pellizzeri. Maximum likelihood signal processing techniques to detect a step pattern of change in multitemporal SAR images. *IEEE Transactions on Geoscience and Remote Sensing*, 40(4):853–870, 2002.
- [4] X. Su, C.A. Deledalle, F. Tupin, and H. Sun. NORCAMA: Change analysis in SAR time series by likelihood ratio change matrix clustering. *ISPRS Journal of Photogrammetry and Remote Sensing*, 101:247–261, 2015.
- [5] K. Conradsen, A. A. Nielsen, J. Schou, and H. Skriver. A test statistic in the complex Wishart distribution and its application to change detection in polarimetric SAR data. *IEEE Transactions on Geoscience and Remote Sensing*, 41(1):4–19, 2003.
- [6] K. Conradsen, A.A. Nielsen, and H. Skriver. Determining the points of change in time series of polarimetric SAR data. *IEEE Transactions on Geoscience and Remote Sensing*, 54(5):3007–3024, 2016.
- [7] L. Pulvirenti, M. Chini, N. Pierdicca, and G. Boni. Use of SAR data for detecting floodwater in urban and agricultural areas: The role of the interferometric coherence. *IEEE Transactions on Geoscience and Remote Sensing*, 54(3):1532–1544, 2016.
- [8] M.T. Pham, G. Mercier, and J. Michel. Change detection between SAR images using a pointwise approach and graph theory. *IEEE Transactions on Geoscience and Remote Sensing*, 54(4):2020–2032, 2016.
- [9] G. Quin, B. Pinel-Puysegur, J.M. Nicolas, and P. Loreaux. MIMOSA: An automatic change detection method for SAR time series. *IEEE Transactions on Geoscience and Remote Sensing*, 52(9):5349–5363, 2014.
- [10] S. Lobry, L. Denis, and F. Tupin. Multi-temporal SAR image decomposition into strong scatterers, background, and speckle. *IEEE Journal of Selected Topics in Applied Earth Observations and Remote Sensing*, 9(8):3419–3429, 2016.